Appl. Phys. A 87, 217–221 (2007)
DOI: 10.1007/s00339-006-3824-5

Applied Physics A
Materials Science & Processing

B. HOU[1]
H. WEN[2]
Y. LENG[3]
W. WEN[1,✉]

Enhanced transmission of electromagnetic waves through metamaterials

[1] Department of Physics, the Hong Kong University of Science and Technology, Clear Water Bay, Kowloon, Hong Kong, P.R. China
[2] Department of Electrical and Computer Engineering, the University of British Columbia, Vancouver, Canada
[3] Department of Mechanical Engineering, the Hong Kong University of Science and Technology, Clear Water Bay, Kowloon, Hong Kong, P.R. China

Received: 20 August 2006/Accepted: 15 November 2006
Published online: 30 January 2007 •

ABSTRACT This paper reviews our recent experimental and simulation results regarding the electromagnetic wave transmission through three configurations of sandwiching structures of metamaterials: a metallic mesh sandwiched between two identical layers composed of split rings, metallic fractals, and fractal slits, respectively. We observed the enhanced transmission of the waves through these three types of sandwiching composites with respect to the opaque metallic mesh. The locations of the transmission peaks in the spectrum are associated closely with the band characteristics of the sandwiching layer by appearing either on the left- or the right-hand side of its band.

PACS 41.20.Jb; 42.70.Qs; 78.20.-e; 42.25.Bs; 47.53.+n

1 Introduction

Conventionally, when a beam of light strikes the interface between two optical media at some incidence angle, it will be refracted into another side of the normal when traveling to the other side of the medium. However, a type of new materials, called negative-index materials (NIMs) or left-handed materials (LHMs), has been recently invented and constructed. For this type of media, when the light ray propagates from a conventional medium, e.g. air, to them, the refracted light is bent into the same side of the normal as the incident light, which implies that they have a negative refractive index n [1–4]. The unconventional property of NIMs, based on the simultaneous occurrence of negative permittivity ε and negative permeability μ, was originally conceived by Veselago [5]. Following the pioneering theoretical work done by Pendry et al. [6, 7], Smith and Shelby et al. experimentally demonstrated a negative-index material at microwave-frequency range through constructing the composite medium with periodic arrangements of thin conducting wires and split-ring resonators (SRRs) [8, 9]. Such extraordinary materials are classified as metamaterials, a type of material whose properties are determined solely by its artificially constructed structure rather than by the material it is composed of.

✉ Fax: 852-2358-1652, E-mail: phwen@ust.hk

As another interest of investigation concerning the interactions between electromagnetic (EM) waves and structured materials, the phenomena of enhanced transmissions of EM waves through an opaque medium have received intensive studies in the past few decades, because their underlying physical mechanisms differ significantly from one case to another. For instance, the excitation of surface plasmons was found to induce high transmission of optical waves through a metallic film [10]. Especially, Ebbesen et al. have reported more massive transmission of light through the metal film with two-dimensional arrays of subwavelength holes perforated in it, even if the holes are very small compared with the relevant wavelength [11–14]. Furthermore, the perfect transmission through metallic films with thin slits is observed as a result of induced Fabry–Pérot resonance of propagating waves inside the slits [15–18]. Actually, the earliest experimental demonstration of NIMs is that the composite shows a transmission band in the otherwise opaque EM spectrum of any single negative index permittivity material [8]. This transmission is caused by the appearance of negative n from the simultaneous occurrence of electric resonance in the conducting wires and magnetic resonance in the SRRs.

Very recently, another mechanism, called ABA tunneling, was proposed to enable the transparency of a classically opaque layer B (negative ε) by attaching two identical layers A (high ε) to stimulate an enhancement of magnetic fields at two AB interfaces [19]. Based on the rigorous calculation for a homogeneous medium, such a tunneling transmission effect can be observed in a broad spectrum range, from microwave and infrared to optics and even quantum systems [20]. Although this mechanism requires a carefully selected material index, a metamaterial with its versatile design parameters can facilitate the observation of such an ABA transparency effect, especially in the microwave-frequency range. Therefore, we can employ the novel metamaterials and observe the enhanced microwave transmission through the ABA structures. In this review, we summarize the enhanced transmission phenomena of EM waves through such ABA structured metamaterials.

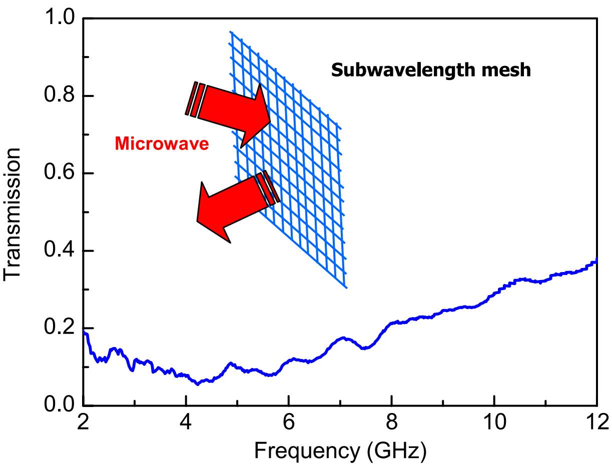

FIGURE 1 The measured transmission of a microwave normally incident upon a metallic mesh sample whose cell measures $5 \times 5\ \mathrm{mm}^2$

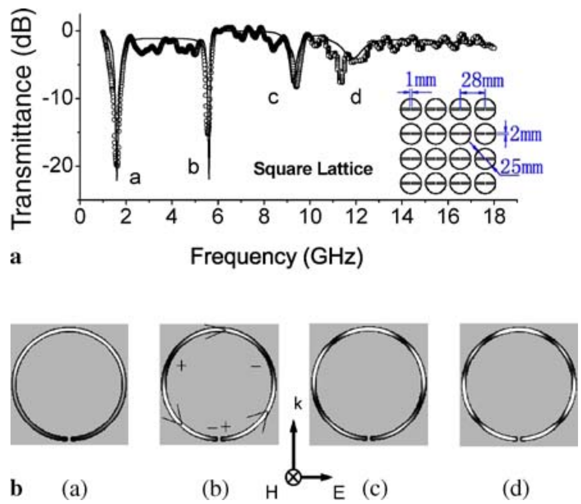

FIGURE 2 (**a**) The transmittance at normal incidence of the plane waves for a square lattice of split rings with E parallel and H perpendicular to the ring plane. The *open circles* denote the experiment and the *solid line* denotes the simulation. (**b**) The distributions of the resonant current amplitude on the ring at frequencies a, b, c, and d, denoted in (**a**). In the *gray-scale plot*, *white* represents maximum amplitude and *black* represents zero amplitude. The background color is irrelevant here; the *black contour* is the exterior of the ring; the *arrow* indicates the current direction at an instantaneous moment; the *positive and negative signs* denote the charges

2 Experiments and results

It is well known that a subwavelength metallic mesh can be modeled as a negative-ε medium, and thus blocks the EM wave propagation effectively. Figure 1 shows the low transmission within 2–12 GHz for a mesh sample whose unit cell measures $5 \times 5\ \mathrm{mm}^2$. In our study, we regarded such a metallic mesh as layer B, and found that placing two identical layers A composed of metamaterials on both sides of the metallic mesh can significantly enhance the transmission of the EM waves through the negative-ε medium (mesh) at certain frequencies, where the transmissions may reach 100% in principle.

2.1 *Structure 1: split ring/mesh/split ring*

First we investigated the stop-band properties of the SRR. It was made from a foam ball, 25 mm in diameter, surrounded by an aluminum ring (width of 2 mm and thickness of 0.1 mm) with an opening gap of 1 mm (see Fig. 2a, inset for detailed geometry) at its equator. SRRs separated by a distance of 28 mm from center to center were affixed to the paper substrate, as shown in Fig. 2a, inset. Two identical double-ridged waveguide horn antennas were connected to the ports of a network analyzer to measure the transmission spectrum of the propagating EM wave. Correspondingly, finite difference time domain simulations were also performed with periodic boundary conditions and the perfect conductor approximation adopted.

We measured and simulated the transmission at normal incidence of the plane waves through the SRR sample; both experimental results and simulations indicate multiple stop bands as appearing in Fig. 2a, and the simulated current distributions on the split ring at these stop frequencies suggest that these bands correspond to different resonant modes of the split ring, see Fig. 2b. The mode with the lowest frequency, referred to as the magnetic resonance, shows a circular current distribution with its maximum amplitude located at the side opposite to the split; furthermore, we found that the resultant band is robust to even a disordered lattice structure. However, the electrical resonances appearing at the higher modes have increasing current nodes along the ring and their band properties are quite sensitive to the configurations of the lattice [21].

Next we took the square lattice of split rings as layer B and observed the normal transmission for the ABA structure, split ring/mesh/split ring, as illustrated in Fig. 3a. In the experiment, each unit of the SRRs is a single square ring with the side of 12.0 mm and the split of 2.0 mm, and was replicated in the x and y directions at a constant 20 mm apart. Two identical layers of the SRRs were attached to both sides of the mesh with a separation distance of s to form a sandwich structure ABA. Interestingly, some transmission peaks were noted when the ABA structure was formed, and these peaks are associated closely with the stop bands of the split rings, which were identified as either magnetic or electrical resonances. Figure 3b shows the experimental results for the normal transmissions of layer A and layer B separately, and the combined layer ABA within the frequency range of 2–12 GHz. When measured individually, layer B reflects most of the incident wave exhibiting low transmission characteristic with the transmittances varying from $\sim 10\%$ to $\sim 40\%$, while layer A allows the microwaves to pass through at most frequencies except for two stop bands at 3.35 and 10.25 GHz. When combined with a separation distance of 0.3 mm between neighboring layers, the sandwiching structure gives rise to a transmission peak ($\sim 30\%$) at 3.74 GHz and a twin peak ($\sim 70\%$) around 9.0–10.0 GHz. Compared to the layer B alone, the introduction of the A layers significantly enhances the transmission of the opaque layer B at these frequencies. In particular, it is noted from the spectra that the first enhanced transmission peak occurs at the right-hand side of the lower-frequency stop band of layer A, while the next twin peak is at the left-hand side of the higher-frequency stop band. As the separation s between adjacent layers increases, the 3.74-GHz peak fades rapidly, while the twin peaks located near 10 GHz

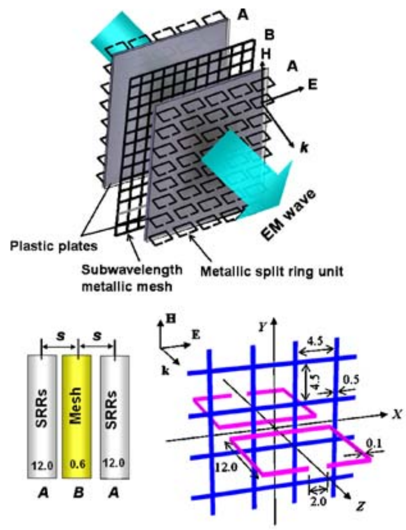

a

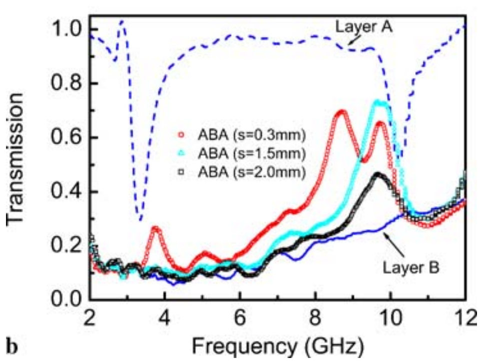

b

FIGURE 3 (**a**) *Upper*: schematic illustration of the sample. *Lower left*: the side view; s denotes the distance separating the layers. *Lower right*: the perspective view of the split unit cell of the sample. The length unit is in millimeters. (**b**) The measured normal transmissions of layers A and B as well as the ABA layers at various separations. The EM waves are incident along the z direction with the electric field polarized along the x axis and the magnetic field along the y axis

become merged into one, remaining at the left-hand side of the stop dip, and then diminish.

According to Pendry et al. [6, 7], the mesh, layer B, has an effective permittivity like

$$\varepsilon_{\mathrm{B}}^{\mathrm{eff}} = \beta_1 - \beta_2^2/f^2 \,, \tag{1}$$

where f denotes the frequency. The negative values of $\varepsilon_{\mathrm{B}}^{\mathrm{eff}}$ spanning the measured frequencies lead to the low transmission through layer B. As for the two stop bands of layer A, their characteristics can be described by the effective media parameters of the Lorentzian profile: an effective permeability at the lower band

$$\mu_{\mathrm{A}}^{\mathrm{eff}} = a_1 + a_2/(3.35^2 - f^2) \,, \tag{2}$$

f in GHz; and an effective permittivity at the higher band

$$\varepsilon_{\mathrm{A}}^{\mathrm{eff}} = \alpha_1 + \alpha_2/(10.25^2 - f^2) \,, \tag{3}$$

f in GHz. For an ABA sandwiching structure as discussed above, the negative ε and μ coexist for the frequencies immediately higher than 3.35 GHz, where the negative branch of $\mu_{\mathrm{A}}^{\mathrm{eff}}$ appears, resulting in the 3.74-GHz minor peak with negative n in nature [8]. On the other hand, the peaks between 8.0 and 10.0 GHz originate from the tunneling mechanism of transmission [19], where the two high-ε slabs facilitate the EM wave to tunnel through a medium with negative permittivity. In this scenario, the SRRs act as the high-ε slabs at the frequencies slightly lower than the electrical resonance frequency 10.25 GHz and facilitate the EM wave to propagate through the layer B without attenuation. The simulation shows that the transmission can reach up to 100% because the early decay of the waves inside the layer B is completely compensated by the growth afterwards [22]. Otherwise, the wave would pass as the evanescent wave only, since the layer B of negative permittivity is a forbidden barrier for EM waves.

2.2 *Structure 2: metallic fractal/mesh/metallic fractal*

A fractal is a type of geometrical structure with self-similarity or scale invariance [23]. Here we introduce a fractal pattern, called an H-fractal, which is a type of space-filling curve and has the fractal dimension of 2. First, the initiator of the fractal is an 'H' with equal height and breadth. Sequentially, four generators, replicating the initiator but being scaled in size by a factor of $1/2$, are attached to free ends of the initiator. This procedure is then repeated, and ultimately the pattern will tile a two-dimensional square with the increasing number of iterations [24, 25]. The metallic H-fractal pattern is easily fabricated by using a shadow-masking/etching process on a standard printed circuit board. Previously, we found that the EM wave transmission spectra through such a metallic H-fractal possess multiple band gaps for the ultra-wide microwave frequency range with these bands being subwavelength [24]. Furthermore, the frequency response of a metallic H-fractal can be attributed to an effective dielectric constant in the form of

$$\varepsilon_{\mathrm{eff}} = \alpha + \sum_l \beta_l/(f_l^2 - f^2) \,, \tag{4}$$

where α and β_l are inputting parameters, f_l is the lth resonant frequency, and the index l runs over all band gaps [24].

Now we replace the split rings with the metallic fractals to construct the sandwiching triple layers, as illustrated in Fig. 4a. Two identical layers A, each composed of a periodic arrangement of metallic fractal patterns, were attached to both sides of the layer B in the same manner as the ABA structure of the SRRs. The measured transmission through layer A reveals three stop bands in the spanned frequency range at 1.3, 2.7, and 7.1 GHz, respectively, as plotted in Fig. 4b. At the left-hand sides of these stop bands, the ABA layers give rise to two transmission peaks, one about 80% at 2.5 GHz and the other about $\sim 60\%$ at about 5.0 GHz. It should be noted that the transmission peaks, similar to the second band in the case of the split rings, are located at the left-hand sides of their corresponding stop bands; such an outcome is expected according to the tunneling transmission theory [19]. The transmission in X polarization shows a similar pattern [26]. In summary, by employing the fractal pattern, we observed multiple transmission enhancements in the same spectrum.

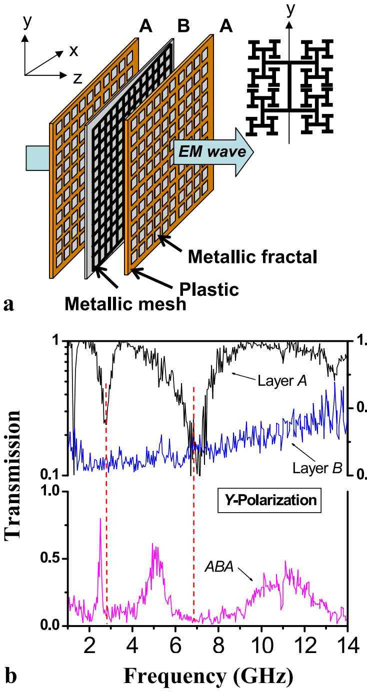

FIGURE 4 (**a**) The schematic picture of the sample. A six-level planar fractal pattern is illustrated in the *top right hand corner*. The planar fractal pattern is periodically replicated in the x–y plane with the first-level line along the y direction. (**b**) The normal transmission spectra of the layers A and B and the combining layer ABA measured under Y polarization. In the *upper panel*, the left-hand axis, logarithmic scale, is for the layer A, and the right-hand one, linear scale, is for the layer B. The *vertical dashed lines* denote the correspondence of the transmission peaks of ABA to the stop bands of layer A

2.3 *Structure 3: fractal slit/mesh/fractal slit*

A fractal slit or aperture is a complementary version of the metallic H-fractal described above. It has been found that the fractal slit exhibits high transmission regardless of its subwavelength scale in all cross-sectional dimensions of the aperture. Phenomenally different from the recently discovered enhanced transmissions via surface plasmon excitations [11–14] and Fabry–Pérot-like resonances [15–18], both of which depend strongly on the sample thickness, the transmission in the fractal-slit case is independent of the incidence angle, plate thickness, or array periodicity, and is governed by a transversal shape resonance localized in the slits. In particular, the EM field experiences no phase change when transmitting through the metallic plate wherein the subwavelength fractal slits are arranged periodically [27]. Here we used the fractal slit to clad the metallic mesh and observed the enhanced transmission through the mesh, as illustrated in Fig. 5a.

Figure 5b shows the normal transmissions of EM waves through layers A and B, respectively. The unit cell of layer A is intrinsically a 10-level fractal structure, wherein the slot etched on the copper plate has the width of 0.2 mm and the first-level length of 10 mm. It is observed that layer A reflects the wave at most frequencies except for some pass bands, located at 1.8, 4.0, and 10.2 GHz, where almost 100% transmittances could be reached. The two pass bands, appearing at the lower frequencies (longer wavelengths) 1.8 and 4.0 GHz in the plot, indicate a type of unusual subwavelength transmission, since the ~ 167 mm wavelength of an EM wave penetrated through layer A was more than one order of magnitude greater than the length of the longest slit (10 mm). This transmission is attributed to the local resonance induced inside the fractal slits [27]. Conclusively, this type of ABA structure exhibits multiple transmission peaks located at the right-hand sides of the pass bands of the bare layer A. The same phenomena occur for another polarization [26].

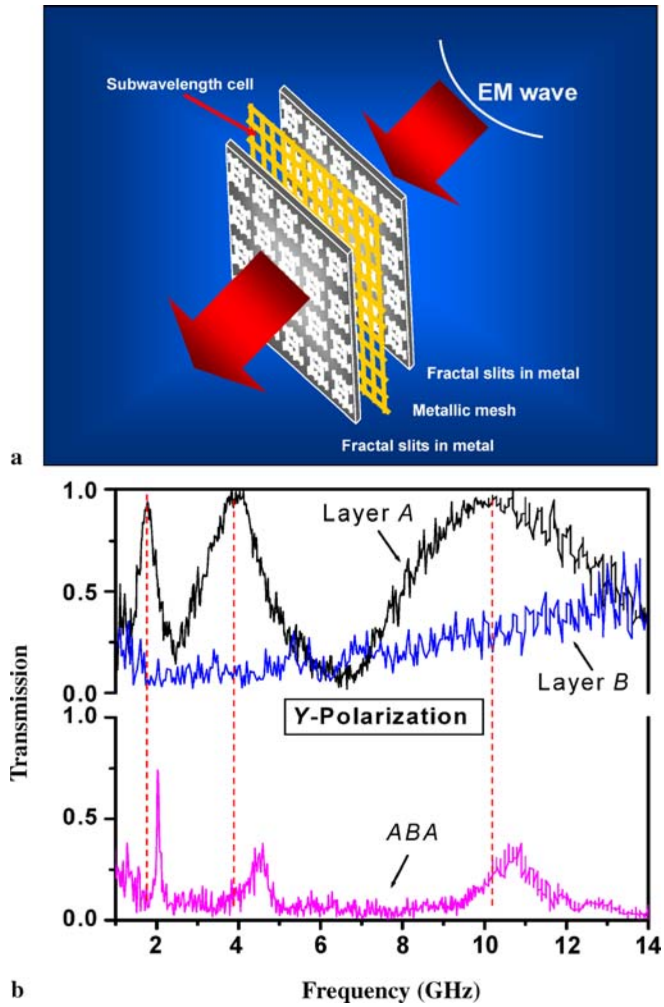

FIGURE 5 (**a**) The schematic picture of the sample. (**b**) The normal transmission spectra of the layers A and B and the combining layer ABA measured under Y polarization. The *vertical dashed lines* denote the correspondence of the transmission peaks of ABA to the pass bands of layer A

A comparison between the sandwiching structures 2 and 3 shows different transmission characteristics. For the former, the ABA transmission peaks are located to the left of layer A's bands; while, for the latter, the peaks are located to the right. We speculate that the reason for the differing behaviors of the two ABA sandwich structures is that the layer A's bands in 2 and 3 are formed as a result of the different nature of the resonances. For the metallic fractal, its stop bands are induced by the electrical resonances. For the fractal slit, which is the inverted structure to the metallic fractal, its pass bands can be attributed to the excitation of a magnetic resonance with the magnetic current induced in the slots, according to Babinet's principle [28]. Therefore, the change in the nature of the resonance from electrical in the H-strips to magnetic in the H-slits causes the transmission peak of the composite ABA to shift from the left-hand side of layer A's band to the right-hand side.

3 Conclusion

We investigated the EM wave transmission through three configurations of sandwiching structures of metamaterials, and observed the enhanced transmission with respect to the opaque metallic mesh after being sandwiched between two identical layers composed of split rings, metallic fractals, and fractal slits, respectively. The locations of the transmission peaks are closely associated with the band characteristics of the sandwiching layer by appearing either on the left- or the right-hand side of it. For the layered metamaterials discussed in this review, the enhanced transmission may be attributed to the coupling of local resonances induced in the two sandwiching layers, theorized as a valid homogeneous medium. Therefore, it is possible to observe the transparency of a metallic mesh over a broad frequency band through properly integrating differently sized metamaterial elements which have their bands connecting together into the sandwiching layers. Such a composite might find applications in radar detection and antenna design. Furthermore, considering the wave nature of electrons in quantum mechanics, it is desirable to explore the corresponding transmission (tunneling) of electrons through quantum systems similar to the photonic sandwiching structures.

ACKNOWLEDGEMENTS The authors are thankful to Mei Jun and Qiu Cunyin for beneficial discussions. This project is supported by Hong Kong RGC grants CA02/03.SC01 and HKUST603603.

REFERENCES

1 J.B. Pendry, D.R. Smith, Phys. Today **57**, 37 (2004)
2 J.B. Pendry, Contemp. Phys. **45**, 191 (2004)
3 D.R. Smith, J.B. Pendry, M.C.K. Wiltshire, Science **305**, 788 (2004)
4 S.A. Ramakrishna, Rep. Prog. Phys. **68**, 449 (2005)
5 V.G. Veselago, Sov. Phys. Uspekhi **10**, 509 (1968)
6 J.B. Pendry, A.J. Holden, W.J. Stewart, I. Youngs, Phys. Rev. Lett. **76**, 4773 (1996)
7 J.B. Pendry, A.J. Holden, D.J. Robbins, W.J. Stewart, IEEE Trans. Microw. Theory Technol. **47**, 2075 (1999)
8 D.R. Smith, W.J. Padilla, D.C. Vier, S.C. Nemat-Nasser, S. Schultz, Phys. Rev. Lett. **84**, 4184 (2000)
9 R.A. Shelby, D.R. Smith, S. Schultz, Science **292**, 77 (2001)
10 R. Dragila, B. Luther-Daviers, S. Vukovie, Phys. Rev. Lett. **55**, 1117 (1985)
11 T.W. Ebbesen, H.J. Lezec, H.F. Ghaemi, T. Thio, P.A. Wolff, Nature **391**, 667 (1998)
12 H.F. Ghaemi, T. Thio, D.E. Grupp, T.W. Ebbesen, H.J. Lezec, Phys. Rev. B **58**, 6779 (1998)
13 L. Martín-Moreno, F.J. García-Vidal, H.J. Lezec, K.M. Pellerin, T. Thio, J.B. Pendry, T.W. Ebbesen, Phys. Rev. Lett. **86**, 1114 (2001)
14 W.L. Barnes, W.A. Murray, J. Dintinger, E. Devaux, T.W. Ebbesen, Phys. Rev. Lett. **92**, 107 401 (2004)
15 J.A. Porto, F.J. García-Vidal, J.B. Pendry, Phys. Rev. Lett. **83**, 2845 (1999)
16 H.E. Went, A.P. Hibbins, J.R. Sambles, C.R. Lawrence, A.P. Crick, Appl. Phys. Lett. **77**, 2789 (2000)
17 F. Yang, J.R. Sambles, Phys. Rev. Lett. **89**, 063 901 (2002)
18 F.I. Baida, D.V. Labeke, G. Granet, A. Moreau, A. Belkhir, Appl. Phys. B **79**, 1 (2004)
19 L. Zhou, W. Wen, C.T. Chan, P. Sheng, Phys. Rev. Lett. **94**, 243 905 (2005)
20 I.R. Hooper, T.W. Preist, J.R. Sambles, Phys. Rev. Lett. **97**, 053 902 (2006)
21 Y. Qi, B. Hou, W. Wen, J. Phys. D Appl. Phys. **38**, 590 (2005)
22 B. Hou, H. Wen, Y. Leng, W. Wen, Appl. Phys. Lett. **87**, 201 114 (2005)
23 M. Barnsley, *Fractals Everywhere* (Academic, San Diego, CA, 1988)
24 W. Wen, L. Zhou, J. Li, W. Ge, C. Chan, P. Sheng, Phys. Rev. Lett. **89**, 223 901 (2002)
25 W. Wen, Z. Yang, G. Xu, Y. Chen, L. Zhou, W. Ge, C.T. Chan, P. Sheng, Appl. Phys. Lett. **83**, 2106 (2003)
26 H. Wen, B. Hou, Y. Leng, W. Wen, Opt. Express **13**, 7005 (2005)
27 W. Wen, L. Zhou, B. Hou, C.T. Chan, P. Sheng, Phys. Rev. B **72**, 153 406 (2005)
28 B.A. Munk, *Frequency Selective Surfaces, Theory and Design* (Wiley, New York, 2000)